J|A|C|S ARTICLES

Published on Web 09/09/2009

Continuous-Wave and Pulsed EPR Characterization of the [2Fe−2S](Cys)$_3$(His)$_1$ Cluster in Rat MitoNEET

Toshio Iwasaki,*,† Rimma I. Samoilova,‡ Asako Kounosu,† Daijiro Ohmori,§ and Sergei A. Dikanov*,||

Department of Biochemistry and Molecular Biology, Nippon Medical School, Sendagi, Bunkyo-ku, Tokyo 113-8602, Japan, Institute of Chemical Kinetics and Combustion, Russian Academy of Sciences, Novosibirsk 630090, Russia, Department of Chemistry, Juntendo University, Inba, Chiba 270-1695, Japan, and Department of Veterinary Clinical Medicine, University of Illinois at Urbana-Champaign, Urbana, Illinois 61801

Received April 22, 2009; E-mail: tiwasaki@nms.ac.jp; dikanov@illinois.edu

Abstract: CW EPR spectra of reduced [2Fe−2S](Cys)$_3$(His)$_1$ clusters of mammalian mitoNEET soluble domain appear to produce features resulting from the interaction of the electron spins of the two adjacent clusters, which can be explained by employing the local spin model. This model favors the reduction of the outermost iron with His87 and Cys83 ligands, which is supported by orientation-selected hyperfine sublevel correlation (HYSCORE) characterization of the uniformly ^{15}N-labeled mitoNEET showing one strongly coupled nitrogen from the His87 N$_\delta$ ligand with hyperfine coupling $^{15}a = 8$ MHz. The ^{14}N and ^{15}N HYSCORE spectra also exhibit at least two different cross-peaks located near diagonal in the (++) quadrant, with frequencies ∼2.8 and 2.4 MHz (N2), and the other ∼4.0 and 3.5 MHz (N1), but did not show any of the larger splitting ∼1.1−1.4 MHz previously seen with Rieske proteins. Further analysis with partially ^{15}N(3)-His-labeled protein indicates that His87 N$_\varepsilon$ cross-peaks produce resolved features (N2) in the ^{14}N spectrum but contribute much less than weakly coupled peptide nitrogen species to the (++) quadrant in the ^{15}N spectrum. It is suggested that these quantitative data may be used in future functional and theoretical studies on the mammalian mitoNEET [2Fe−2S] cluster system.

Introduction

"MitoNEET" is the mammalian mitochondrial outer membrane protein[1] found as a possible target protein by cross-linking with a photoaffinity derivative of pioglitazone.[2] This drug is a member of the thiazolidinedione class of insulin sensitizers for treatment of type II diabetes, viz., the complex metabolic disease characterized by insulin resistance in the initial stage.[3] Deficiency of mitoNEET expression in mice results in a compromise in the respiratory capacity of cardiac mitochondria.[1] Recent 1.5−1.8-Å structures of the recombinant soluble (CDGSH-type zinc finger-like) domain of human mitoNEET have revealed that the mitoNEET soluble domain (rec mitoNEET) is a homodimer with each subunit binding a unique [2Fe−2S] cluster (but no Zn^{2+}) in a three-cysteine plus one-histidine ligand environment (Figure 1a).[4−6] Although the integrity of a [2Fe−2S] cluster and the functional role of the His87 ligand in native mitoNEET in vivo remains unknown, its thermophilic bacterial water-soluble homologue from *Thermus thermophilus* HB8 has been overproduced in *Escherichia coli*, crystallized, and found to contain two adjacent mitoNEET-like [2Fe−2S]-(Cys)$_3$(His)$_1$ clusters per dimeric unit.[7] These results indicate the presence of the redox-active, mitoNEET-like dimeric [2Fe−2S](Cys)$_3$(His)$_1$ protein family across various organisms from thermophiles to mammals.[7] Interest in the redox chemistry and physiology of the mitoNEET superfamily has been heightened by the recent availability of crystal structures[4−6] (Figure 1a). However, information about the electronic structure and interaction of this novel "twin" [2Fe−2S] cluster system is currently very limited, and the site of iron reduction and the cluster's magnetic interaction with the protein environment which account for the electron transfer function and mechanism have remained elusive.

Strong antiferromagnetic coupling between the electron spins of two irons via a bridging structure produces an EPR-silent ($S = 0$) ground state in the oxidized $Fe^{3+}-Fe^{3+}$ form of the [2Fe−2S] cluster and a paramagnetic $S = {}^1/_2$ ground state in the reduced $Fe^{3+}-Fe^{2+}$ form. Thus, the reduced cluster in frozen solution is characterized by the anisotropic EPR spectrum,

† Nippon Medical School.
‡ Russian Academy of Sciences.
§ Juntendo University.
|| University of Illinois at Urbana-Champaign.

(1) Wiley, S. E.; Murphy, A. N.; Ross, S. A.; van der Geer, P.; Dixon, J. E. *Proc. Natl. Acad. Sci. U.S.A.* **2007**, *104*, 5318–5323.
(2) Colca, J. R.; MacDonald, W. G.; Waldon, D. J.; Leone, J. W.; Lull, J. M.; Bannow, C. A.; Lund, E. T.; Mathews, W. R. *Am. J. Physiol. Endocrinol. Metab.* **2004**, *286*, E252–E260.
(3) Wiederkehr, A.; Wollheim, C. B. *Endocrinology* **2006**, *147*, 2643–2649.
(4) Lin, J.; Zhou, T; Ye, K.; Wang, J. *Proc. Natl. Acad. Sci. U.S.A* **2007**, *104*, 14640–14645.
(5) Paddock, M. L.; Wiley, S. E.; Axelrod, H. L.; Cohen, A. E.; Roy, M.; Abresch, E. C.; Caprarp, D.; Murphy, A. N.; Nechushtai, R.; Dixon, J. E.; Jennings, P. A. *Proc. Natl. Acad. Sci. U.S.A.* **2007**, *104*, 14342–14347.
(6) Hou, X.; Liu, R.; Ross, S.; Smart, E. J.; Zhu, H.; Gong, W. *J. Biol. Chem.* **2007**, *282*, 33242–33246.
(7) Kounosu, A.; Iwasaki, T.; Baba, S.; Hayashi-Iwasaki, Y.; Oshima, T.; Kumasaka, T. *Acta Crystallogr., Sect. F* **2008**, 1146–1148.

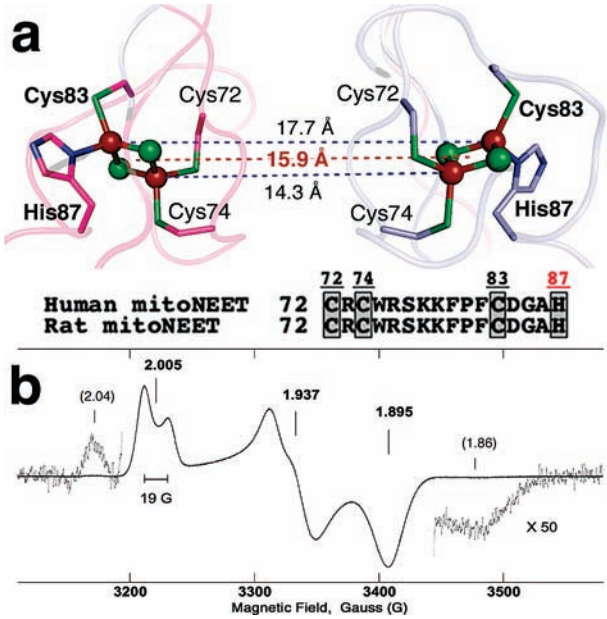

Figure 1. (a) Relative location of two clusters in the human rec mitoNEET dimeric structure (2QH7.pdb). In this structure, the outermost iron is coordinated by solvent-exposed His87 and Cys83 ligands, and the innermost iron is coordinated by Cys74 and Cys72 ligands.[4−6] (b) X-band CW EPR spectrum of reduced rat rec mitoNEET at 20 K. Additional weak wings, probably resulting from magnetic interaction of the reduced clusters, accompany the main EPR signal on the high and low field sides (unaccounted for the qualitative analysis in the main text). Microwave frequency and power, 9.037 GHz and 0.01 mW; sample concentration, ∼4 mM (per protomer).

typically as a result of a rhombic **g**-tensor. The distinguishing feature between the reduced plant ferredoxin $[2Fe-2S](Cys)_4$ and Rieske $[2Fe-2S](Cys)_2(His)_2$ clusters is the average value of the **g**-tensor components g_{av}, which is ∼1.96 for plant ferredoxins and ∼1.91 for Rieske proteins.[8] The cluster in the mitoNEET protein family is the first example of a redox-active [2Fe−2S] cluster with asymmetrical coordination of one of the irons (Figure 1). Before the discovery of the mitoNEET protein family we had rationally engineered a $[2Fe-2S](Cys)_3(His)_1$ environment into the hyperthermophilic archaeal Rieske-type ferredoxin (ARF) scaffold of *Sulfolobus solfataricus* (DDBJ-EMBL-GenBank code, AB047031) with replacement of the His64→Cys ligand (H64C-ARF). This accommodated a fairly thermostable [2Fe−2S] cluster in the oxidized form.[9] However, its high sensitivity to dithionite reduction even under anaerobic conditions (leading to irreversible reductive cluster breakdown) precluded detailed characterization of its reduced state.[9] Thus, rec mitoNEET opens a new path to explore a deeper analysis of the paramagnetic form of a unique $[2Fe-2S](Cys)_3(His)_1$ cluster. We herein report the continuous-wave (CW) and two-dimensional pulsed EPR (hyperfine sublevel correlation, HYSCORE) characterization of the rat rec mitoNEET (residues 32−108; NCBI_GeneID code 294362) with two nominally identical $[2Fe-2S](Cys)_3(His)_1$ clusters per dimer, providing the first information about the electronic structure in its reduced ground state and peculiarities of the cluster's magnetic interaction with the protein environment.

Experimental Section

Materials. *Escherichia coli* strain JM109 (TaKaRa, Japan) used for cloning was grown in Lauria-Bertani (LB) medium, with 50 μg/mL kanamycin when required. Water was purified by a Millipore Milli-Q purification system. Other chemicals mentioned in this study were of analytical grade.

Sample Preparation. MitoNEET was named on the basis of its subcellular location on the *mito*chondrial outer membrane and the internal amino acid sequence stretch of the mice and human proteins, Asn-Glu-Glu-Thr (*NEET*).[2] A portion of the *cisd1* gene coding for the water-soluble domain (residues 32−108) of *Rattus norvegicus* (rat) mitoNEET (rec mitoNEET) was amplified by polymerase chain reaction (PCR), using the Rat Heart QUICK-Clone cDNA (Lot no. 7060097; Clontech Laboratories, Inc.) and sets of the following PCR primers (designed based on the reported nucleotide sequences): 5′-GGG CCC GCT AGC AGC GGA AAG AAG TTC TAC GCT AAA GAG-3′ and 5′-GGG CCC CTC GAG TTA AGT TTC TTT TTT CTT GAT GAT CAG-3′. The PCR primers included six extra bases (coding for an engineered Ser-Gly linker) immediately upstream of the AAG codon for Lys32 (underlined in the primer sequence above) of the target gene. The amplified PCR product was digested with *NheI* and *XhoI*, and then inserted into an *NheI/XhoI* site of the pET28a vector (Novagen). The resultant vector was named pET28a-RmNEETSG. The pET28a-RmNEETSG vector was transformed into the host strain, *E. coli* CodonPlus(DE3)-RIL (Stratagene), and used for the following EPR sample preparations.

For preparation of the ^{14}N(N/A, 99.63%)-rec mitoNEET sample, the transformants were grown overnight at 25 °C in LB medium containing 50 μg/mL kanamycin, 0.4 mM $FeCl_3$, 0.2 mM L-cysteine hydrochloride monohydrate (Wako Pure Chemicals, Tokyo, Japan), and 1 mg/L pyridoxal hydrochloride (Sigma), and the recombinant holoprotein was overproduced with 1 mM isopropyl β-D-thiogalactopyranoside for 24 h at 22 °C. The cells were pelleted by centrifugation, and the rec mitoNEET (residues 32−108) having a hexahistidine-tag plus a thrombin cleavage site was purified essentially as reported previously for archaeal Rieske [2Fe−2S] proteins and the *Thermus thermophilus* homologue of mammalian mitoNEET,[7,9,10] except that the entire purification was performed at 4 °C using buffers adjusted at pH 8.0 and that the heat treatment of the crude cell lysate was omitted. The sample was further purified by gel-filtration chromatography (Sephadex G-75; Amersham Pharmacia Biotech) eluted at room temperature with 10 mM HEPES-NaOH buffer, pH 8.0, containing 500 mM NaCl, and then concentrated with Centriprep-10 and Microcon-YM10 apparatus (Amicon) to ∼4 mM (per protomer), rapidly frozen in liquid nitrogen, and stored at −80 °C until use.

For preparation of the uniformly ^{15}N-labeled rec mitoNEET sample, the transformants were grown overnight at 25 °C in the CHL-^{15}N (∼97 atm%) medium (Chlorella Industry Co. Ltd., Fukuoka, Japan) containing 50 μg/mL kanamycin, 0.4 mM $FeSO_4$, and vitamin mixture (final concentrations, 5 mg/L of thiamine and 1 mg/L each of biotin, choline hydrogen tartrate, folic acid, niacinamide, D-pantothenate, and pyridoxal), and the recombinant holoprotein was overproduced with 0.5 g/L Algal ^{15}N(98.7−99.2%)-Amino Acid Mix (Chlorella Industry Co. Ltd., Fukuoka, Japan) and 1 mM isopropyl β-D-thiogalactopyranoside for 24 h at 22 °C. In our hands, this system was handy and suitable for heterologous overproduction of the uniformly ^{15}N-labeled iron−sulfur holoproteins by employing the combination of a pET28a vector (Novagen) plus *E. coli* CodonPlus(DE3)-RIL host strain (Stratagene) system, with a higher protein yield (roughly ∼3−5 fold) compared with

(8) Guigliarelli, B.; Bertrand, P. *Adv. Inorg. Chem.* **1999**, *47*, 421–497.
(9) Kounosu, A.; Li, Z.; Cosper, N. J.; Shokes, J. E.; Scott, R. A.; Imai, T.; Urushiyama, A.; Iwasaki, T. *J. Biol. Chem.* **2004**, *279*, 12519–12528.
(10) Iwasaki, T.; Kounosu, A.; Kolling, D. R. J.; Crofts, A. R.; Dikanov, S. A.; Jin, A.; Imai, T.; Urushiyama, A. *J. Am. Chem. Soc.* **2004**, *126*, 4788–4789.

our previous overproduction procedures using the combinations of the pTrc99A vector/*E. coli* CodonPlus(DE3)-RIL host strain/M9 salt-based synthetic medium system.[9,11] The cells were pelleted by centrifugation, and the uniformly ^{15}N-labeled holoprotein was purified as described above for the nonlabeled protein.

For preparation of the partially ^{15}N(3)-His-labeled rec mitoNEET sample [on the ^{14}N(N/A)-protein background], the transformants were grown overnight at 25 °C in the nonlabeled CHL medium (Chlorella Industry Co. Ltd., Fukuoka, Japan) containing 50 μg/mL kanamycin, 0.4 mM $FeSO_4$, and vitamin mixture (final concentrations, 5 mg/L of thiamine and 1 mg/L each of biotin, choline hydrogen tartrate, folic acid, niacinamide, D-pantothenate, and pyridoxal), and the recombinant holoprotein was overproduced with 0.5 g/L nonlabeled Algal Amino Acid Mix (Chlorella Industry Co. Ltd., Fukuoka, Japan), ~20 mg/L L-histidine/HCl/H_2O (^{15}N(3), 98%) (Cambridge Isotope Laboratories, Inc., Andover, MA) [~10-fold enrichment of L-^{15}N(3)-histidine over intrinsic L-^{14}N(N/A)-histidine (~2 mg/L) in the nonlabeled Algal Amino Acid Mix (which depends on each lot of the commercial Chlorella-derived amino acid mixture and therefore needs to be adjusted)], and 1 mM isopropyl β-D-thiogalactopyranoside for 24 h at 22 °C. In our hands, this method was handy because the histidine auxotrough strain from the *E. coli* CodonPlus(DE3)-RIL derivatives was unavailable to us. The cells were pelleted by centrifugation, and the partially ^{15}N(3)-His-labeled holoprotein was purified as described above for the nonlabeled protein. The two-pulse electron spin−echo envelope modulation (ESEEM) amplitude was used to estimate the efficiency of substitution of the coordinated His87 $^{14}N_\delta$ by ^{15}N in the purified protein sample (~30% in the present case; data not shown).

The uniformly ^{15}N-labeled, recombinant archaeal Rieske-type ferredoxin (ARF; DDBJ-EMBL-GenBank code, AB047031) from the hyperthermoacidophile *Sulfolobus solfataricus* strain P1 was prepared as reported previously.[9] Dithionite-reduced Rieske-type [2Fe−2S] cluster in wild-type ARF shows the typical EPR spectrum from a rhombic **g**-tensor, with principal values $g_z = 2.02$, $g_y = 1.90$, $g_x = 1.81$.[9] In the (++) quadrant of the ^{15}N HYSCORE spectrum measured near g_z, the uniformly ^{15}N-labeled ARF showed at least two superimposed but well-resolved pairs of the cross-peaks at (1.7, 1.2) MHz ($^{15}N_\varepsilon$) and (2.0, 0.92) MHz ($^{15}N_p$) with the splittings of 0.5 and 1.1 MHz, respectively (see Figure 4d).

EPR and ESEEM Experiments. CW X-band EPR spectra were measured at 9.8−50.4 K by using a JEOL X-band JES-FA300 spectrometer equipped with an ES-CT470 Heli-Tran cryostat system and a Scientific Instruments digital temperature indicator/controller model 9700.

Pulsed EPR measurements were carried out using an X-band Bruker ELEXSYS E580 spectrometer with an Oxford CF 935 cryostat at 10−11 K.

ESEEM experiments with two pulse and 2D four-pulse sequences were employed, with appropriate phase cycling schemes to eliminate unwanted features from experimental echo envelopes. In the two-pulse electron spin echo (ESE) experiment ($\pi/2$-τ−π-τ echo), the intensity of the echo signal after the second pulse is recorded as a function of time, τ. In the 2D four-pulse experiment ($\pi/2$-τ−$\pi/2$-t_1−π-t_2−$\pi/2$-τ echo, also called hyperfine sublevel correlation, HYSCORE), the intensity of the stimulated echo after the fourth pulse was measured with variation of t_2 and t_1 while τ remained constant. The length of a $\pi/2$ pulse was nominally 16 ns and a π pulse was 32 ns. The repetition rate of pulse sequences was 1000 Hz. HYSCORE data were collected in the form of 2D time-domain patterns containing 256 × 256 points with a step 20 or 32 ns. Spectral processing of ESEEM patterns, including subtraction of relaxation decay (fitting by polynoms of 3−4 deg), apodization (Hamming window), zero filling, and fast Fourier transformation (FT), was performed using Bruker WIN-EPR software.

Nitrogen ESEEM and HYSCORE spectra were analyzed as described in Supporting Information.

Results and Discussion

CW EPR Spectrum and Analysis of Spin−Spin Interactions between Two [2Fe−2S] Clusters in rec MitoNEET. CW X-band EPR spectrum of the dithionite-reduced, rat rec mitoNEET at pH 8 possesses an anisotropic line shape with a width of ~250 G, corresponding to rhombic **g**-tensor (Figure 1b). The principal values of the **g**-tensor can be estimated by the values $g_z = 2.005$, $g_y = 1.937$, and $g_x = 1.895$. The average value of these components ($g_{av} \approx 1.945$) is reasonably between the values of the plant ferredoxin (~1.96) and Rieske (~1.91) [2Fe−2S] clusters. In addition, EPR spectrum shows the splitting ~19 G of the g_z component in the low field of the spectrum and a broadening of the central g_y component from the poorly resolved splitting of the order ~10 G (Figure 1b). These features resulted from the interaction of the electron spins of two adjacent, reduced clusters in the dimeric unit (Figure 1). This interaction was not recognized in the previously published spectrum of the reduced rec mitoNEET.[12]

X-ray crystal structure of the human rec mitoNEET gives distances of 14.3 and 17.7 Å between the innermost and outermost iron pairs of two [2Fe−2S] clusters, respectively (Figure 1a).[4−6] The distance between the geometrical centers of the two clusters is 15.9 Å. The parameter $D = g^2\beta^2/r^3 = 18500/r^3$ (D in G, r in Å),[13] which characterizes an order of spin−spin interaction between two reduced clusters in the approximation considering them as two $S = {}^1/_2$ dipoles, varies within the interval 7.7 and 3.3 G for these distances (4.6 G for the center). Thus, the observed large g_z splitting ~19 G (Figure 1b) *cannot* be explained by the simple dipole−dipole interaction of two $S = {}^1/_2$ spins separated by the reported crystallographic distance (~14 to 18 Å) of the two adjacent clusters (Figure 1a).

The EPR spectrum of the reduced rec mitoNEET is more adequately described by employing the "local spin model" which considers the interaction of all four iron spins (two $S = 2$ and two $S = {}^5/_2$) with each other taking into account their relative location.[8,14,15] According to this model the interaction of two [2Fe−2S] clusters with *collinear* Fe(III)−Fe(II) vectors can be replaced by two $S = {}^1/_2$ dipoles with an effective distance r_{eff} described by the equation:

$$r_{\mathrm{eff}}{}^{-3} = \sum_{i,j} K_i K_j r_{ij}{}^{-3} \qquad i = 2(\mathrm{Fe(II)}), 3(\mathrm{Fe(III)}); \quad j = 2(\mathrm{Fe(II)}), 3(\mathrm{Fe(III)}) \quad (1)$$

where $K_{i(j)} = {}^7/_3$ for Fe(III) and $K_{i(j)} = -{}^4/_3$ for Fe(II).

One can extend this approach in the case of arbitrary orientation of the applied magnetic field relative to two clusters with symmetrical location, as found in the rec mitoNEET structure (Figures 1a and 2a). Let us define vectors $\mathbf{r}_{22}$ and $\mathbf{r}_{33}$ connecting the Fe(II)$_A$−Fe(II)$_B$ and Fe(III)$_A$−Fe(III)$_B$ in clusters A and B, respectively (Figure 2a). The $\mathbf{r}_{22}$ and $\mathbf{r}_{33}$ are parallel

(11) Iwasaki, T.; Kounosu, A.; Uzawa, T.; Samoilova, R. I.; Dikanov, S. A. *J. Am. Chem. Soc.* **2004**, *126*, 13902–13903.

(12) Wiley, S. E.; Paddock, M. L.; Abresch, E. C.; Gross, L.; van der Geer, P.; Nechushtai, R.; Murphy, A. N.; Jennings, P. A.; Dixon, J. E. *J. Biol. Chem.* **2007**, *282*, 23745–23749.

(13) Parmon, V. N.; Kokorin, A. I.; Zhidomirov, G. M. *J. Magn. Reson.* **1977**, *28*, 339–349.

(14) Bertrand, P.; More, C.; Guigliarelli, B.; Fournel, A.; Bennett, B.; Howes, B. J. *J. Am. Chem. Soc.* **1994**, *116*, 3078–3086.

(15) More, C.; Asso, M.; Roger, G.; Guigliarelli, B.; Caldeira, J.; Moura, J.; Bertrand, P. *Biochemistry* **2005**, *44*, 11628–11635.

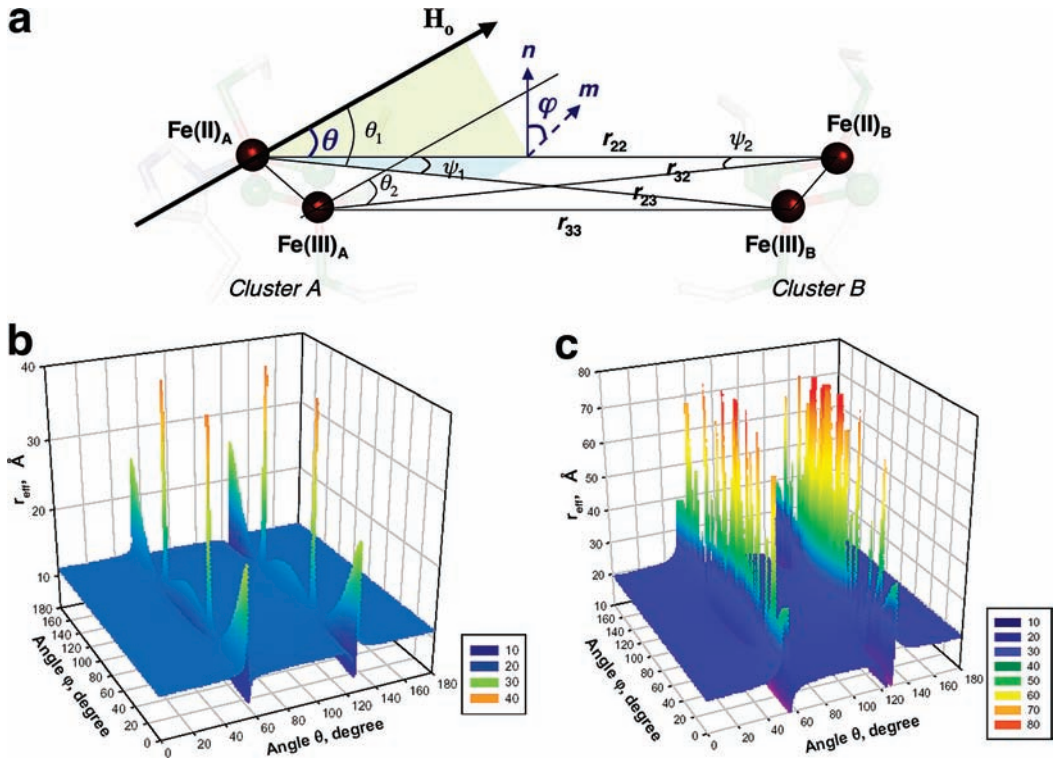

Figure 2. Schematic presentation of vectors and angles described in the text (a). In this figure, the $\mathbf{r}_{22}$ and $\mathbf{r}_{33}$ form the same angle θ with the external magnetic field vector $\mathbf{H}_o$. φ is the angle between the planes containing the vectors ($\mathbf{r}_{23}$,$\mathbf{r}_{22}$) and ($\mathbf{r}_{22}$,$\mathbf{H}_o$) and is equal to that between their normals **n** (to the plane containing $\mathbf{r}_{23}$ and $\mathbf{r}_{22}$) and **m** (to the plane containing $\mathbf{r}_{22}$ and $\mathbf{H}_o$). The deviation of **m** from **n** depends on the orientation of $\mathbf{H}_o$. The r_{eff} distance (Å) calculated as a function of angles θ and φ (with the step 1°) when the *outermost* iron pair (b) or the *innermost* iron pair (c) undergoes the reduction in rec mitoNEET (in 3D presentation). The contour presentation of these graphs (b,c) is given in Figure S2 in Supporting Information.

to each other and form the same angle θ with the magnetic field vector $\mathbf{H}_o$. In contrast, the vectors $\mathbf{r}_{23}$ and $\mathbf{r}_{32}$, connecting $Fe(II)_A-Fe(III)_B$ and $Fe(III)_A-Fe(II)_B$, respectively, form the angles θ_1 and θ_2 with the vector $\mathbf{H}_o$. These angles could be described through the angle θ as[16]

$$\cos\theta_{1,2} = \cos\theta\cos\psi_{1,2} + \sin\theta\sin\psi_{1,2}\cos\varphi \qquad (2)$$

where $\psi_{1,2}$ is the angle between $\mathbf{r}_{ii}$ and $\mathbf{r}_{ij}$ or $\mathbf{r}_{ji}$, ($i,j = 2,3$), and φ is the angle between the planes containing the vectors ($\mathbf{r}_{ij}$,$\mathbf{r}_{ii}$) and ($\mathbf{r}_{ii}$,$\mathbf{H}_o$). Because of the symmetrical cluster location, the angles $\psi_{1,2}$ are related to each other as $\psi_1 = -\psi_2 = \psi$.

The interaction between four iron atoms from two reduced [2Fe−2S] clusters in the approximation neglecting the difference in the **g**-tensor anisotropy of different centers is characterized by the sum

$$\sum_{i,j} K_i K_j r_{ij}^{-3}(1 - 3\cos^2\theta_{ij}) \qquad i = 2,3; \quad j = 2,3 \qquad (3)$$

This sum could be rewritten in the explicit form as

$$S_{dd} = (49/9)(1/r_{33})^3(1 - 3\cos^2\theta) + (16/9)(1/r_{22})^3(1 - 3\cos^2\theta) - (28/9)[(1/r_{23})^3(1 - 3\cos^2\theta_1) + (1/r_{32})^3(1 - 3\cos^2\theta_2)] \qquad (4)$$

Our aim is to replace the four terms in the equation above by one term, which would effectively describe these interactions by the interaction of two $S = {}^1/_2$ spins, which are separated by the distance r_{eff} between two similar points on the lines coming through Fe(II) and Fe(III) of each [2Fe−2S] cluster. Because of symmetry reasons, the line connecting these points should be parallel to the $Fe(II)_A-Fe(II)_B$ and $Fe(III)_A-Fe(III)_B$ lines, and form the same angle θ with applied magnetic field, that is, the sum S_{dd} should be replaced by the term

$$S_{dd} = r_{eff}^{-3}(1 - 3\cos^2\theta) \qquad (5)$$

The particular value of the sum S_{dd} depends on which iron site in the cluster is reduced. If one suggests that the outermost iron pair (with His87 and Cys83 ligands; Figures 1a and 2a) undergoes the reduction, then the distances between irons in the eq 4 are equal to $r_{33} = 14.3$ Å, $r_{22} = 17.7$ Å; $r_{23}(r_{32}) = 16.14$ Å. In the opposite case with the innermost iron pair (with Cys 74 and Cys72 ligands; Figure 1a) they are $r_{22} = 14.3$ Å, $r_{33} = 17.7$ Å; $r_{23}(r_{32}) = 16.14$ Å. The published crystallographic coordinates of the iron atoms in the clusters A and B in rec mitoNEET[4−6] allow one to calculate the angle ψ, which is equal to 7.5° assuming an ideal planar geometry of the clusters.

Figure 2 panels b and c show calculated distance r_{eff} as a function of angles θ and φ for the cases of the outermost and innermost iron reduction, respectively, when the r_{eff} for these cases is described by the expressions

$$r_{eff} = 10/(2.18 - 0.74z_1 - 0.74z_2)^{1/3} \qquad (6)$$

$$r_{eff} = 10/(1.58 - 0.74z_1 - 0.74z_2)^{1/3}$$

where

$$z_1 = (1 - 3\cos^2\theta_1)/(1 - 3\cos^2\theta) \quad \text{and}$$

$$z_2 = (1 - 3\cos^2\theta_2)/(1 - 3\cos^2\theta)$$

(16) Shubin, A. A.; Dikanov, S. A. *J. Magn. Reson.* **1983**, *52*, 1–12.

Our calculations demonstrate that the "local spin" interactions of four irons in rec mitoNEET could be effectively described by the interaction of two spin $S = {}^1/_2$ located at the effective distance $r_{\text{eff}} \sim 11$ Å (for most orientations of the magnetic field relative to the molecular axes of the cluster defined by angles θ and φ), when the *outermost* iron is reduced (Figure 2b). In the opposite case with reduction of the innermost iron, the effective distance r_{eff} is substantially longer: ~22 Å (Figure 2c).

The parameter D, defined above, is equal to ~13 G for the r_{eff} distance ≈ 11 Å. This distance is sufficient to produce the splitting ~19 G observed in the EPR spectra (Figure 1b), because the dipole−dipole splitting of the g_i component, which is equal to ${}^3/_2D(1 - 3\cos^2\theta_i)$, could change from ${}^3/_2D$ to $-3D$.[13,17] In this expression, $\cos^2\theta_i$ is the direction cosines of the dipole−dipole axis relative to the principal axes of the **g**-tensor. It is reasonable to assume that the g_z splitting resolved in the EPR spectrum (Figure 1b) corresponds to the angle θ_z close to ~90°. On the other hand, the r_{eff} distance ~22 Å is even longer than the real distances between iron atoms and would lead to even *smaller* couplings. Hence the present qualitative analysis suggests that the *outermost* iron pair with His87 and Cys83 ligands is reduced in the mixed-valent state of the mitoNEET [2Fe−2S] cluster (Figure 1).

In the qualitative analysis described above, two additional considerations must be given. First, the presence of $(1 - 3\cos^2\theta)$ in the denominator of z_1 and z_2 in eq 6, which suggests a division on "0" when θ is equal to the magic angle 54.7° (or 125.3°) (see Supporting Information, Figure S2). In this case, the spin−spin interaction is equal to zero for the Fe(II)−F(II) and Fe(III)−Fe(III) pairs but it is not zero for Fe(II)−Fe(III) pairs. For fixed θ and ψ, the value of the sum S_{dd} (and spin−spin splitting) would depend on the angle φ. The remaining interaction between Fe(II)−Fe(III) pairs could be characterized by the sum S_{dd} varying from 2.8×10^{-5} to -2.3×10^{-5} Å^{-3} for φ changing from 0° to 90° (or from 180° to 90°). These S_{dd} values are substantially smaller than the cases when the spin−spin interaction is not zero for the Fe(II)−Fe(II) and Fe(III)−Fe(III) pairs [e.g., for two considered cases of the reduction when the magnetic field is normal to all $\mathbf{r}_{ij}$ vectors (i.e., $\theta = \theta_1 = \theta_2 = 90°$) and the r_{eff} distance is equal to 11.3 and 21.5 Å, the sum S_{dd} is equal to 7×10^{-4} and 1×10^{-4} Å^{-3}, respectively]. Thus, when θ is equal to the magic angle, the interaction between Fe(II)−Fe(III) pairs would not produce observable splittings in the EPR spectrum.

Second, the particular spin−spin splitting for the magnetic field oriented along each principal axis is determined by its orientation which is defined in the considered model by the angles θ and φ. The selection of the principal directions for the [2Fe−2S] cluster is usually based on symmetry constraints. Thus, the three directions naturally related to the cluster geometry, which is very close to planar, are often considered as the principal direction of the **g**-tensor, and include the directions coinciding with the Fe−Fe and S−S vectors and the vector normal to the cluster plane. It should be noted however that theoretical considerations, DFT calculations as well as indirect analysis by powder ENDOR of biological [2Fe−2S] clusters in ferredoxins and Rieske proteins have given somewhat confusing contradictions in the assignment of g_{max}, g_{mid}, and g_{min} principal axes along particular molecular directions.[18] Moreover, the single-crystal EPR study on the reduced Rieske cluster in the crystalline cytochrome bc_1 complex with the stigmatellin in the Q_o-site has demonstrated that the **g**-tensor principal axes are indeed *skewed* with respect to the molecular directions of the [2Fe−2S] core by up to 30°−40°.[19] This finding implies that the protein environment significantly disturbs the electronic structure of the cluster, because any model, based on an ideal crystal field with ideal C_{2v} symmetry from the liganding atoms of the Fe(II), would fail to predict such an effect. The situation is even more uncertain with the rec mitoNEET case, where the initial symmetry constraint is apparently not applicable because of the mixed ligation of the outermost iron site.[4−6] Thus, complete analysis of the interaction between two clusters in rec mitoNEET would require extensive EPR spectral simulation considering the interaction between four iron atoms with the geometry provided by the crystal structure, more detailed knowledge about the (probably skewed) orientation of the **g**-tensor axes within the molecular frame of the clusters, and knowledge about possible weak exchange interaction between these clusters.[8,14,15] The previous studies on analogous biological metalloenzyme systems have proven a certain effectiveness of the multifrequency EPR approach for providing additional restrictions on the parameters varying in simulations,[15] and such studies are being planned in our laboratories.

^{14}N and ^{15}N HYSCORE Characterization of the Hyperfine and Quadrupole Couplings from Directly Coordinated Nitrogen. Reduction of the outermost iron pair with His87 and Cys83 ligands in the mixed-valent state of the mitoNEET [2Fe−2S] cluster, indicated by local spin model analysis, can be addressed independently by the ESEEM/HYSCORE characterization of hyperfine (**HF**) couplings from directly coordinated nitrogen of the His87 ligand. The representative ^{14}N HYSCORE spectrum of the reduced ^{14}N(N/A)-rec mitoNEET is shown in Figure 3a. It consists of two quadrants containing cross-peaks from several nitrogens. Previous analysis with different values of ^{14}N **HF** couplings[20,21] allows us to assign extended cross-peaks in the (+−) quadrant to strongly coupled (coordinated) $^{14}N_\delta$ of the histidine ligand (His87), and two pairs of cross-peaks in the (++) quadrant with an approximately circular shape of small radius to other, nonliganding nitrogens.

The HYSCORE spectra taken at the low and high extreme edges near the maximal and minimal **g** values (e.g., Figure 3a) give "single-crystal-like" patterns from the reduced clusters, whose g_z and g_x axes are directed along the magnetic field, despite the spin−spin interaction of the two clusters. This is because the addition of the local magnetic field ~20 G induced by the spin−spin interaction to the vector of external magnetic field ~3300 G would give only insignificant deviation of the total magnetic field vector (less than 1°). The cross-peaks from N_δ (nuclear spin $I = 1$) determine two sets of nuclear frequencies from $m_s = \pm 1/2$ manifolds. For instance, in the (+−) quadrant of the g_x spectrum (Figure 3a), the most intense cross-peaks at [±9.0; ∓4.6] MHz (dd) are assigned to the dq−dq correlation from strongly coupled His87 N_δ, based on the difference between two dq frequencies (close to $4\nu_I$ of ^{14}N), their contour line shape, and their intensities.[20] N_δ also produces well-

(17) Gulin, V. I.; Dikanov, S. A.; Tsvetkov, Yu. D. *Chem. Phys. Lett.* **1990**, *170*, 211–216.
(18) Shubin, A. A.; Dikanov, S. A. *Appl. Magn. Reson.* **2006**, *30*, 399–416.
(19) Bowman, M. K.; Berry, E. A.; Roberts, A. G.; Kramer, D. M. *Biochemistry* **2004**, *43*, 430–436.
(20) Dikanov, S. A.; Xun, L.; Karpiel, A. B.; Tyryshkin, A. M.; Bowman, M. K. *J. Am. Chem. Soc.* **1996**, *118*, 8408–8416.
(21) Dikanov, S. A.; Shubin, A. A.; Kounosu, A.; Iwasaki, T.; Samoilova, R. I. *J. Biol. Inorg. Chem.* **2004**, *9*, 753–767.

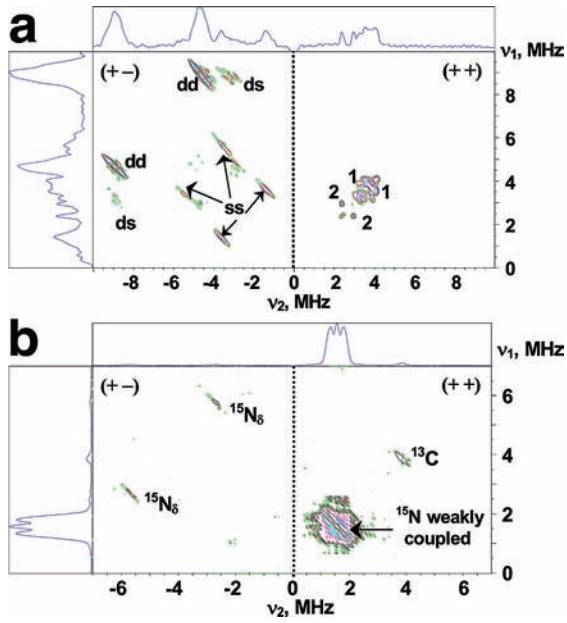

Figure 3. HYSCORE spectra in contour presentation of the reduced [2Fe−2S] cluster in ^{14}N(N/A, 99.63%) (a) and uniformly ^{15}N-labeled (b) rat rec mitoNEET; dd, ds, and ss are cross-peaks correlating d, double-quantum, and s, single-quantum transitions. Magnetic field, time τ, and microwave frequency were 3672 G, 136 ns, 9.706 GHz (a); 3580 G, 136 ns, 9.704 GHz (b).

pronounced dq−sq peaks [±9.0; ∓3.2] MHz (ds), which correlate the dq_+-transition 9.0 MHz with the sq-frequency of ∼3.2 MHz from the same manifold as the dq_--transition with 4.6 MHz. The cross-peaks (dd) and (ds) determine one set of nuclear frequencies ∼(4.6, 3.2, 1.4) MHz with quadrupole splitting $3|Q_z| \cong 0.18$ MHz (see equation s1 in Supporting Information). Assuming the same quadrupole contribution to the sq-frequencies, a second nuclear triplet was determined with frequencies of ∼(9.0, 5.4, 3.6) MHz. This set of frequencies in two-manifolds is supported by the cross-peaks [±5.4; ∓3.2] and [±3.6; ∓1.4] MHz in the (+−) quadrant (Figure 3a).

Similarly, in the g_z spectrum, the dq−dq correlations at [±8.4; ∓4.6] MHz (dd) and the dq−sq peaks at [±8.4; ∓2.2] MHz (ds) define nuclear set (∼4.6, 2.4, 1.4) MHz with $3|Q_z| \cong 0.2$ MHz (Figure S2a in Supporting Information). The frequencies from the opposite manifold were then estimated to be ∼(8.4, 4.3, 4.1) MHz. This assignment is supported by the cross-peaks [±4.3; ∓2.2] and [±4.0; ∓2.4] MHz in the (+−) quadrant and [±4.3; ∓2.2] MHz in the (++) quadrant, which are located in the typical frequency region of the sq−sq transitions (Figure S3a in Supporting Information).

The central EPR peak with maximal intensity formally corresponds to the $g_y = 1.937$ principal value of the g-tensor, but the spectra recorded at this field position are not "single-crystal-like". Despite the partial powder character, HYSCORE spectra measured at this position (Figure S3b in Supporting Information) consist of well-resolved cross-peaks and contain dq−dq correlations [±8.4; ∓4.3] MHz (dd), as well as a dq−sq correlation [±8.4; ∓3.0] MHz (ds) defining nuclear sets in two manifold as (4.3, 3.0, 1.3) MHz and (8.4, 5.0, 3.4) MHz. These sets are also supported by the sq−sq correlations in the (++) and (+−) quadrants (Figure S3b in Supporting Information).

The $^{14}N_\delta$ nuclear frequencies from the His87 ligand, determined from the HYSCORE spectra recorded at the fields corresponding to principal values of the **g**-tensor, provide an estimate of diagonal components of the **HF** and quadrupole tensors in the **g**-tensor coordinates (using the equations s1−s3 in Supporting Information) and the isotropic **HF** constant $^{14}a = 6.1$ MHz. These results are summarized in Tables 1−3.

The ^{15}N HYSCORE spectrum of the uniformly ^{15}N-labeled rec mitoNEET (Figure 3b) shows only one pair of cross-peaks in the (+−) quadrant from the His87 $^{15}N_\delta$ (nuclear spin $I = {}^1/_2$, no quadrupole moment). The isotropic and anisotropic parts of axial **HF** tensor $^{15}a = 8$ MHz, $^{15}T = 1.1$ MHz (corresponding to $^{14}a = 5.7$ MHz and $^{14}T = 0.8$ MHz) defining principal values of the tensor were given by the contour line shape analysis (see

Table 1. Nuclear Frequencies of the Coordinated His87 N_δ in rec mitoNEET and Calculated **HF** and Quadrupole Couplings at the Fields Corresponding to the Canonical Orientations of the **g**-Tensor[a]

	(g_z)	(g_x)	(g_y)
nuclear frequencies	∼(4.6, 2.4, 2.2)	∼(4.6, 3.2, 1.4)	∼(4.3, 3.0, 1.3)
at g_i[b] (MHz)	∼(8.4, 4.3, 4.1)	∼(9.0, 5.4, 3.6)	∼(8.4, 5.0, 3.4)
$3\|Q_i\|$[b] (MHz)	∼0.2	∼1.8	∼1.7
ν_I[c] (MHz)	1.06	1.13	1.11
A_{1i}[b,d] (MHz)	6.3, 6.7	6.7, 6.9	6.2, 6.5
A_i[b,e] (MHz)	5.9	6.6	5.9

[a] The position of the isolated peak in the HYSCORE spectra was affected by the value of time τ and by the accuracy of the frequency measurement from the discrete character of the 2D data acquisition. These two factors produce an error in the determination of the cross-peak maximum of the order ∼0.1 MHz. Therefore, the frequencies reported above and couplings derived from them are determined with accuracies not less than this error. [b] $i = x, y, z$; $3|Q_z|$, $3|Q_x|$, $3|Q_y|$ are the quadrupole couplings along g_z, g_x, g_y principal directions of **g**-tensor. [c] ν_I = ^{14}N Zeeman frequency for the corresponding HYSCORE spectra measured at g_z, g_x, or g_y point of the EPR spectrum (Figure 1). [d] A_{1z}, A_{1x}, A_{1y} = **HF** couplings determined from each dq transition of the two opposite manifolds using the first-order equation 9 in Supporting Information. [e] A_z, A_x, A_y = second-order corrected **HF** couplings determined from both of the dq frequencies using the equation 11 in Supporting Information. Thus, A_{iso} (isotropic **HF** coupling calculated as $(A_z + A_x + A_y)/3$) is 6.1 MHz (6.1 MHz for $^{14}N_\delta$ corresponds to 8.5 MHz for $^{15}N_\delta$).

Table 2. Comparison of the ^{14}N **HF** Couplings (MHz) near Canonical Directions of the **g**-Tensor in rec mitoNEET, SDX[a], and ARF[a]

	A_z	A_x	A_y	A_{iso}
His87 N_δ in rec mitoNEET	**5.9**	**6.6**	**5.9**	**6.1**
$N_\delta(1)$ in SDX[b]	4.7	4.7	4.3	4.6
$N_\delta(2)$ in SDX[b]	**6.1**	**5.0**	**5.1**	**5.4**
$N_\delta(1)$ in ARF[b]	4.5	4.3	4.2	4.4
$N_\delta(2)$ in ARF[b]	**5.9**	**5.2**	**5.1**	**5.4**

[a] SDX is a high-potential, archaeal Rieske protein called sulredoxin from *Sulfolobus tokodaii* with a weak homology to the cytochrome *bc*-associated Rieske proteins;[10,11,21,39] ARF is a low-potential, archaeal homologue of an oxygenase-associated Rieske-type ferredoxin from *S. solfataricus*[9,10,21] (see Figure 4d). [b] Data taken from ref 21. The N_δ **HF** tensors in Rieske-type proteins depend on anisotropic interaction with the electron spins of the Fe(II) and Fe(III), and the spin density transferred onto the strongly coupled (i.e., coordinated) $^{14}N_\delta$ atom. The constrains on N_δ location (stable Fe−N_δ distances and angles between Fe−Fe and Fe−N_δ) based on the available crystal structures would account for the similarity of **HF** tensors between different proteins, if they are determined mainly by the location of the N_δ nuclei relative to the electron spins of the cluster, and are relatively insensitive to variations in orientation of the imidazole plane. The latter influences only the overlap of the iron and nitrogen orbitals responsible for the spin density transfer onto the ligand. This means that the **HF** tensor of the strongly coupled N_δ and its principal directions mainly reflect the position of the nitrogen atom itself relative to the iron−sulfur cluster, and therefore would not provide direct information about changes in orientation of the imidazole plane, so long as the N_δ location remains approximately constant.[21]

Table 3. Comparison of the ^{14}N Nuclear Quadrupole Couplings (MHz) near Canonical Directions of the **g**-Tensor in rec mitoNEET, SDX[a] and ARF[a]

	(g_z)	(g_x)	(g_y)
His87 N_δ in rec mitoNEET	~0.2	~**1.8**	~1.7
$N_\delta(1)$ in SDX[b]	**1.4**	1.0	0.9
$N_\delta(2)$ in SDX[b]	**1.8**	~1.2	1.1
$N_\delta(1)$ in ARF[b]	**1.6**	0.4	0.5
$N_\delta(2)$ in ARF[b]	**1.6**	1.5	0.9

[a] SDX is a high-potential, archaeal Rieske protein called sulredoxin from *S. tokodaii* with a weak homology to the cytochrome *bc*-associated Rieske proteins;[10,11,21,39] ARF is a low-potential, archaeal homologue of an oxygenase-associated Rieske-type ferredoxin from *S. solfataricus*[9,10,21] (see Figure 4d). [b] Data taken from ref 21. The principal directions of the nuclear quadrupole tensor are determined by the geometry of the electron orbitals around the nucleus, and are associated with the ligand molecule itself. For instance, the principal directions of the nuclear quadrupole interaction tensor for the N_δ imine nitrogen of the imidazole ring are retained if this nitrogen is coordinated to the metal, and thus could be used for the characterization of the ligand orientation in the metal−imidazole complex of interest.[21]

Supporting Information, Figure S1).[22] Notably, these parameters for His87 N_δ in rec mitoNEET are only ~10% above the corresponding values for one of the two N_δ values (with larger **HF** tensor) in Rieske-type proteins (Table 2). This provides the second indication that the Fe^{2+} site in the reduced cluster of rec mitoNEET is the *outermost* iron.

On the other hand, maximum **HF** and quadrupolar splittings from $^{14}N_\delta$ in rec mitoNEET are observed along $g_{x(\min)}$ axis, in contrast to the $g_{z(\max)}$ axis for both nitrogens in Rieske-type proteins (SDX/ARF)[21] (underlined in Tables 2 and 3). The **HF** tensor of the directly coordinated N_δ and its principal directions mainly reflect the position of the nitrogen atom itself relative to the iron−sulfur cluster, whereas the principal directions of the *nuclear quadrupole interaction* tensor are determined by the geometry of the electron orbitals around the nucleus and are associated with the ligand molecule itself. Both cluster types have one common N_δ ligand located at the equivalent position relative to the [2Fe−2S] cluster (as judged by similar Fe−N_δ distances, angles between the Fe−Fe and Fe−N_δ, and orientations of imidazole plane), which would account for the similar **HF** and quadrupole tensors (Tables 2 and 3). On the basis of these considerations, we suggest a possible difference in orientation of the g_{max}, g_{mid}, and g_{min} principal axes of the **g**-tensors relative to the basic molecular axes between the mitoNEET and Rieske cluster systems.

Weakly Coupled (Noncoordinated) Nitrogens N1 and N2 in the ^{14}N(N/A)-rec MitoNEET Spectra. Previously published data have indicated that the protonated N_ε-H of the noncoordinated imidazole and histidine ring possesses a characteristic nuclear quadrupole coupling constant $K = e^2qQ/4h = \sim 0.35$ MHz and a high asymmetry parameter $\eta = 0.915-0.995$ [for comparison, nonprotonated imine nitrogen possesses $K \approx 0.81-0.84$ MHz and $\eta = 0.13$, leading to a quadrupole parameter $\kappa = K^2(3 + \eta^2) = \sim 2$ MHz^2].[23−25] Only slight variations of the quadrupole coupling constant ($K \approx 0.35-0.43$ MHz) have been reported for the amine N_ε in metal complexes of imidazole coordinated via N_δ,[26−29] which are substantially lower than the typical values ($K \approx 0.75-0.85$ MHz) previously reported for the peptide nitrogens (N_p).[30−35] Thus, if the strongly coupled nitrogen is from the directly coordinated N_δ nucleus of a histidine ligand, it should be accompanied by a weaker coupling from the noncoordinated remote N_ε of the histidine imidazole ring, with its quadrupole coupling constant K reflecting the protonation/deprotonation status of N_ε. In many metalloproteins and in model complexes, the isotropic **HF** coupling of the directly bound nitrogen of histidine or imidazole has been shown to be ~20 times that of the remote nitrogen.[11,35−38]

In the ^{14}N(N/A)-rec mitoNEET system, there are two pairs of nonextended (circular shape) cross-peaks **1** and **2** in the ^{14}N HYSCORE spectra located closely to diagonal of the (++) quadrant due to small difference in the correlated frequencies (Figures 3a and 4a). Their frequencies are [4.08; 3.5] MHz and [2.86; 2.32] MHz, respectively, when recorded at the g_y region. Similar cross-correlations were observed in the same area when measured near g_z and g_y, even though the correlated frequencies vary within several tenths of MHz.

Because a broad set of orientations contributes to the g_y spectrum, it seems appropriate to estimate the nitrogen couplings using approaches developed for the orientation disordered systems. We suggest that the closely located cross-peaks in the (++) quadrant (see Figures 3a and 4a) correlate two transitions of maximum frequency ν_{dq+} and ν_{dq-} from opposite manifolds of two different nuclei N1 and N2, respectively. In this case an application of formal expressions for the frequency of double-quantum transitions

$$\nu_{dq\pm} = 2[\nu_{ef\pm}{}^2 + \kappa]^{1/2} \quad (7)$$

where the effective nuclear frequency in each manifold $\nu_{ef\pm}$, given by $\nu_{ef\pm} = |\nu_I \pm |A|/2|$, and the quadrupole parameter $\kappa = K^2(3 + \eta^2)$ would provide an estimate of the **HF** coupling A from the ^{14}N of interest:

$$A = (\nu_{dq+}{}^2 - \nu_{dq-}{}^2)/8\nu_I \quad (8)$$

This equation gives $^{14}A = 0.32$ MHz for N2 in the g_y spectrum (Zeeman frequency $\nu_I = 1.1056$ MHz) that corresponds to 0.448

(22) Dikanov, S. A.; Bowman, M. K. *J. Biol. Inorg. Chem.* **1998**, *3*, 18–29.
(23) Edmonds, D. T.; Summers, C. P. *J. Magn. Reson.* **1973**, *12*, 134–142.
(24) Hunt, M. J.; Mackay, A. L.; Edmonds, D. T. *Chem. Phys. Lett.* **1975**, *34*, 473–475.
(25) Hunt, M. J.; Mackay, A. L. *J. Magn. Reson.* **1976**, *22*, 295–301.
(26) Ashby, C. I. H.; Cheng, C. P.; Brown, T. L. *J. Am. Chem. Soc.* **1978**, *100*, 6057–6063.
(27) Mims, W. B.; Peisach, J. *J. Chem. Phys.* **1978**, *69*, 4921–4930.
(28) Jiang, F.; McCracken, J.; Peisach, J. *J. Am. Chem. Soc.* **1990**, *112*, 9035–9044.
(29) Colaneri, J.; Peisach, J. *J. Am. Chem. Soc.* **1992**, *114*, 5335–5341.
(30) Edmonds, D. T.; Speight, P. A. *Phys. Lett.* **1971**, *A 34*, 325–326.
(31) Blinc, R.; Mali, M.; Osredkar, R.; Seliger, J.; Ehrenberg, L. *Chem. Phys. Lett.* **1974**, *28*, 158–159.
(32) Ashby, C. I. H.; Paton, W. F.; Brown, T. I. *J. Am. Chem. Soc.* **1980**, *102*, 2990–2998.
(33) Rabbani, S. R.; Edmonds, D. T.; Gosling, P.; Palmer, M. H. *J. Magn. Reson.* **1987**, *72*, 230–237.
(34) Dikanov, S. A.; Tyryshkin, A. M.; Felli, I.; Reijerse, E. J.; Hüttermann, J. *J. Magn. Reson., Ser. B* **1995**, *108*, 99–102.
(35) Dikanov, S. A.; Kolling, D. R. J.; Endeward, B.; Samoilova, R. I.; Prisner, T. F.; Nair, S. K.; Crofts, A. R. *J. Biol. Chem.* **2006**, *281*, 27416–27425.
(36) Mims, W. B.; Peisach, J. In *Advanced EPR: Applications in Biology and Biochemistry*; Hoff, A. J., Ed.; Elsevier: Amsterdam, The Netherlands, 1989; pp 1−57.
(37) Dikanov, S. A.; Samoilova, R. I.; Smieja, J. A.; Bowman, M. K. *J. Am. Chem. Soc.* **1995**, *117*, 10579–10580.
(38) Yeagle, G. J.; Gilchrist, M. L.; McCarrick, R. M.; Britt, R. D. *Inorg. Chem.* **2008**, *47*, 1803–1814.
(39) Iwasaki, T.; Kounosu, A.; Samoilova, R. I.; Dikanov, S. A. *J. Am. Chem. Soc.* **2006**, *128*, 2170–2171.

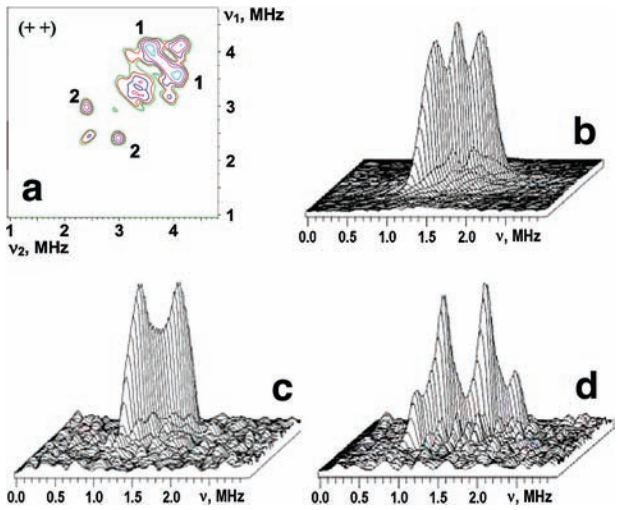

Figure 4. The (++) quadrant of the ^{14}N HYSCORE spectrum taken from Figure 3a (a); 3D stacked presentation of the line from weakly coupled ^{15}N nuclei in the (++) quadrant of ^{15}N HYSCORE spectrum (recorded near g_y) from Figure 3b (b); the same as panel b for uniformly ^{15}N-labeled, reduced rat mitoNEET (c); and a low-potential, archaeal Rieske-type ferredoxin (ARF) from *S. solfataricus* (d). Both panels c and d were recorded near g_z area of the EPR line. Magnetic field, time τ, and microwave frequency, respectively: 3450 G, 136 ns, 9.704 GHz (c); 3425 G, 136 ns, 9.690 GHz (d). Notably, the intensity of the central "matrix" peak at the diagonal point ($^{15}\nu_N$,$^{15}\nu_N$) is suppressed in panels c and d in contrast with panel b (see Figure 5).

MHz for ^{15}N nucleus (Figures 3a and 4a). Substitution of this coupling to the eq 7 gives $\kappa = 0.44$ MHz^2, leading to an estimate for the quadrupole coupling constant $K = e^2qQ/4h = \sim 0.33$ to 0.38 MHz for N2 when η varies between 0 and 1 ($0 \le \eta \le 1$). This K value for N2 (Figure 4a) is consistent with that expected for the protonated imidazole nitrogen.[23−29]

A similar procedure gives the following values for two other frequencies [4.08; 3.5] MHz for N1 (Figures 3a and 4a): $^{14}A =$ 0.5 MHz, (0.7 MHz for ^{15}N), $\kappa = 2.32$ MHz^2, $K = 0.76-0.88$ MHz. This K value for N1 (Figure 4a) is in line with a peptide nitrogen carrying unpaired spin density transferred via the N−H···S type hydrogen bond(s) and/or covalent bond(s) from the reduced [2Fe−2S] cluster.[30−35]

^{14,15}N HYSCORE Analysis of the Selectively ^{15}N(3)-Histidine-Labeled rec MitoNEET. The (++) quadrant of the ^{15}N HYSCORE spectrum (Figure 3b) exhibits an intense triplet of lines from weakly coupled nitrogens including the central peak at ($^{15}\nu_N$,$^{15}\nu_N$) and two other lines around a diagonal point with maximum at [1.77; 1.31] MHz (Figure 4b) corresponding to the **HF** coupling $^{15}A = 0.46$ MHz. Similar coupling at ∼0.4 to 0.5 MHz is found in all spectra measured across the EPR line (Figure 4c). Such spectra for the weakly coupled nitrogens are in stark contrast with the ^{15}N-labeled Rieske protein spectra, which usually show at least two well-resolved splittings 1.1−1.2 MHz (assigned to N_p) and 0.3−0.4 MHz (assigned to remote N_ε of histidine ligand(s))[11,35,39] (Figure 4d).

To directly resolve the coupling from the $^{15}N_\varepsilon/^{15}N_p$ of the His87 ligand, we have attempted to prepare selectively ^{15}N(3)-His-labeled rec mitoNEET [on the ^{14}N(N/A)-protein background] (Figure S4 in Supporting Information). HYSCORE spectra of this sample contain cross-peaks from $^{14,15}N_\delta$ in the (+−) quadrant with dominant contribution of ^{14}N peak (not shown). The two-pulse ESEEM amplitude showed ∼30% substitution of the coordinated $^{14}N_\delta$ by ^{15}N (not shown). Consistently, a new well-separated doublet with the splitting ∼0.45−0.55 MHz (and varying width of up to ∼0.2 MHz due to difference in contributing orientations) for weakly coupled ^{15}N appears symmetrically around the diagonal point ($^{15}\nu_N$,$^{15}\nu_N$) in the (++) quadrant of the HYSCORE spectra (Figure S4b). The appearance of this new doublet for ^{15}N is also accompanied by ∼30% decrease in the relative intensity of the cross-peaks **2** ($K = \sim 0.33$ to 0.38 MHz) relative to that of the cross-peaks **1** ($K = \sim 0.76$ to 0.88 MHz) (Figure S4). This coupling, which gives $^{14}A_{(His)}$ ∼0.32 to 0.39 MHz, agrees with the $^{14}A_2$ from the cross-peaks **2** (for N2) in the ^{14}N spectra. Hence, N2 could be assigned as the protonated form of His87 N_ε taking its K value into account. This gave a ratio of ∼19 for the isotropic **HF** couplings for coordinated N_δ and remote N_ε of the H87 ligand in rec mitoNEET, like those reported previously for Rieske clusters and various other systems.[11,35,39] Additionally, the cross-peaks **1** for N1 in the ^{14}N spectra could be attributed to peptide nitrogen(s) (N_p) other than His87 N_α.

Notably, the difference HYSCORE spectra for the weakly coupled ^{15}N's (between the uniformly ^{15}N-labeled and ^{15}N(3)-His-labeled samples), calculated by taking the $^{14,15}N_\delta$ substitution efficiency into account, gave ∼25% contribution of His87 $^{15}N_\varepsilon$ to the amplitude of the major doublet with the splitting ∼0.4 to 0.5 MHz in g_z and g_x areas and less than ∼10% contribution in g_y area (Figure 5). Moreover, the **HF** coupling $^{15}A \approx 0.7$ MHz, corresponding to $^{14}A \approx 0.5$ MHz for N1 (see Supporting Information, Figure S4b), could not be resolved in the difference spectra (Figure 5b,d). These results suggest that ^{15}N ESEEM amplitude in the rec mitoNEET system (Figure 4b,c) is dominantly affected by certain other peptide nitrogens with smaller isotropic but larger anisotropic coupling, that is, those presumably located closer to Fe^{3+} and not giving resolved cross-peaks in the ^{14}N spectra.

Conclusion

CW X-band EPR spectra of the reduced [2Fe−2S]-$(Cys)_3(His)_1$ clusters in rat rec mitoNEET show features resulting from the interaction of the electron spins of the two adjacent clusters. The observed g_z splitting is explained by employing the "local spin model" considering spin−spin interactions between all four irons in reduced clusters. This model favors the reduction of the outermost iron with His87 and Cys83 ligands. These peculiarities suggest that the mammalian mitoNEET might have evolved to conduct rapid intramolecular electron transfer reaction in the dimeric unit. We are looking forward to elucidating the physiological redox functions of this protein family and its potential relation to diabetes in animals.

^{14}N and ^{15}N HYSCORE characterization has not only confirmed the reduction of the outermost iron sites but also assigned the cross-peaks **2** in the ^{14}N spectra as His87 N_ε, which may be of practical use in future functional studies of rec mitoNEET without any need for isotope labeling. Additionally, these analyses suggest marked differences between the mitoNEET and Rieske [2Fe−2S] protein systems in regard to the **g**-tensor orientation and the interaction with weakly coupled N_p nuclei. In contrast to Rieske proteins, we did not detect N_p(s) with **HF** couplings significantly exceeding the $N_{\varepsilon(His)}$ coupling. We suggest it is likely that peptide nitrogens involved in hydrogen-bond formation with the reduced cluster of the mammalian mitoNEET soluble domain carry less spin density than those of Rieske-type proteins, reflecting their structural differences, including configurations of the liganding residues to the reduced cluster. In conjunction with the marked instability of a reduced [2Fe−2S]$(Cys)_3(His)_1$ cluster ratio-

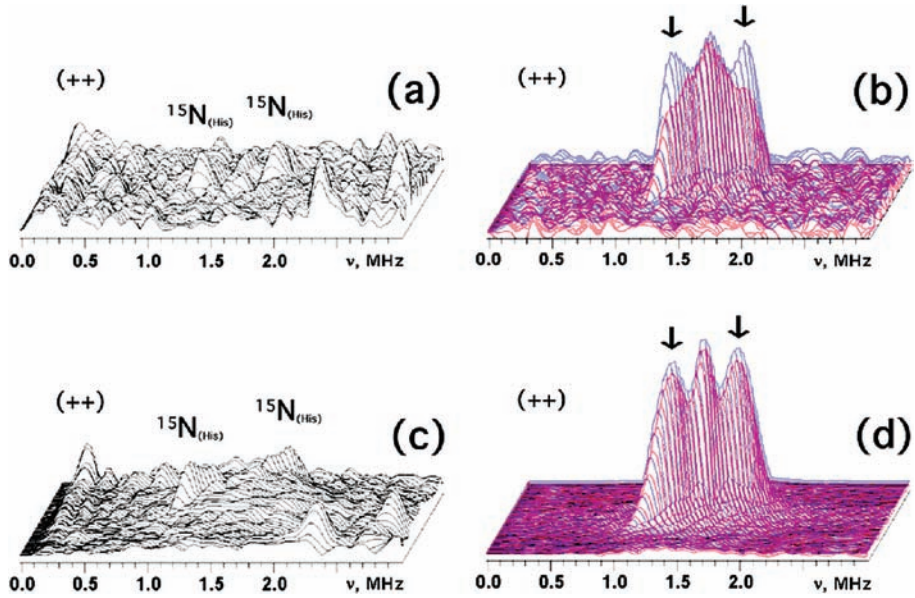

Figure 5. 3D presentation of the HYSCORE spectra in the (++) quadrant of the partially and selectively ^{15}N(3)-His-labeled rec mitoNEET recorded near g_x (a) and g_y (c), and superimposition of the 3D plots for the uniformly ^{15}N-labeled rec mitoNEET (blue) and the difference [uniformly ^{15}N-labeled *minus* ^{15}N(3)-His-labeled rec mitoNEET multiplied by coefficient 3.5 (i.e., corrected for ~30% substitution efficiency for ^{15}N(3)-His)] spectra (red) near g_x (b) and g_y (d). The difference spectra (b,d) indicate ~25% contribution of His87 $^{15}N_\varepsilon$ to the amplitude of major doublet with the splitting ~0.4 to 0.5 MHz in g_x (b) and g_z (not shown) area and less than ~10% contribution in g_y (d) area. This experiment also indicates that scrambling of randomly ^{15}N-labeled peptide and other side chain nitrogens around the cluster does *not* occur with this partially ^{15}N(3)-His-labeled sample (a,c), which would contribute to the central diagonal point ($^{15}\nu_N$,$^{15}\nu_N$) and to areas around this peak in the HYSCORE spectra [as seen with the uniformly ^{15}N-labeled protein (b,d)]. Spectra were recorded at similar conditions with magnetic field 3670 G (near g_x) for panels a and b, and 3580 G (near g_y) for panels c and d; time $\tau = 136$ ns; microwave frequency ≈ 9.70 GHz.

nally engineered into the archaeal Rieske-type ferredoxin scaffold,[9] our results may imply the importance of the cluster's interaction with the protein environment for the assurance of biological redox function. Although the extensive NMR studies on bacterial rubredoxin have revealed some quantitative relations involving unpaired spin density onto peptide nitrogens, strength of hydrogen bonds, and redox properties,[40] NMR identification and full assignment of resonances from a paramagnetic center of a polynuclear iron−sulfur protein with slow electronic relaxation rates (*e.g.* the [2Fe−2S](Cys)$_4$ ferredoxins)[41] are still challenging. Because up to now the parametrization of weakly coupled subsystems has not yet been optimized at the density functional theory level, the present results can also be used in theoretical analysis for selection of an appropriate model of the mixed-valence state of the mammalian mitoNEET system.

Acknowledgment. This investigation was supported by JSPS Grants-in-aid 18608004 (T.I.), 21659111 (T.I.) and 20500628 (D.O.), and by NIH GM062954 Grant (S.A.D.).

Note Added after ASAP Publication. A typographic error in eq 2 in the version published ASAP September 9, 2009, was corrected in the version published September 23, 2009.

Supporting Information Available: Analysis of ^{14}N and ^{15}N ESEEM and HYSCORE spectra, and Figures S1−S4. This material is available free of charge via the Internet at http://pubs.acs.org.

JA903228W

(40) Lin, I.-J.; Gebel, E. B.; Machonkin, T. E.; Westler, W. M.; Markley, J. L. *Proc. Natl. Acad. Sci. U.S.A.* **2005**, *102*, 14581–14586.
(41) Machonkin, T. E.; Westler, W. M.; Markley, J. L. *J. Am. Chem. Soc.* **2004**, *126*, 5413–5426.